REPORT DOCUMENTATION PAGE

Form Approved
OMB No. 0704-0188

1. REPORT DATE *(DD-MM-YYYY)*	2. REPORT TYPE	3. DATES COVERED *(From - To)*
17-07-2013	FINAL PERFORMANCE	01 MAY 2011 - 30 APR 2013

4. TITLE AND SUBTITLE
MULTISCALE MODELING AND MULTIFUNCTIONAL COMPOSITES

5a. CONTRACT NUMBER
FA9550-11-1-0076

5b. GRANT NUMBER

5c. PROGRAM ELEMENT NUMBER

6. AUTHOR(S)
BAHEI-EL-DIN, YEHIA A.

5d. PROJECT NUMBER

5e. TASK NUMBER

5f. WORK UNIT NUMBER

7. PERFORMING ORGANIZATION NAME(S) AND ADDRESS(ES)
THE BRITISH UNIVERSITY IN EGYPT
CAIRO-SUEZ DESERT ROAD
EL-SHOROUK CITY 11837
EGYPT

8. PERFORMING ORGANIZATION REPORT NUMBER

9. SPONSORING / MONITORING AGENCY NAME(S) AND ADDRESS(ES)
AF OFFICE OF SCIENTIFIC RESEARCH
875 N. RANDOLPH ST. ROOM 3112
ARLINGTON VA 22203

10. SPONSOR/MONITOR'S ACRONYM(S)
USAF, AFRL

11. SPONSOR/MONITOR'S REPORT NUMBER(S)

12. DISTRIBUTION / AVAILABILITY STATEMENT
Public Release

13. SUPPLEMENTARY NOTES

14. ABSTRACT

Considering multifunctional fibrous composites, laminates and structures, a unified, transformation field analysis (TFA) approach is developed to model their overall response to thermomechanical loads, as well as local phenomena due to coupled effects and damage. Local stresses and strains generated as a result of piezoelectric and/or pyroelectric behavior of the fibers are treated as transformation fields, which remain in the system even under mechanical unloading. Their effect on the stress and strain distribution at the microscale of a unidirectional composite, the macroscale of a laminate, and the structural scale is determined in terms of transformation influence factors that are a function of the elastic properties of the fiber and matrix phases, and the geometry idealizations at the three length scales. Treatment of damage follows the same scheme but the transformation fields are instead determined such that the local stresses in the affected phase are removed. The result is tri-lengthscale model, which seamlessly connects the stress and strain fields in the fiber and matrix phases, membrane forces and bending moments in laminates, and the overall thermomechanical, structural loads to determine the overall response. The latter is determined with the ABAQUS finite element code, in which the transformation field analysis was implemented.

15. SUBJECT TERMS
COMPOSITES, PIEZOELECTRIC, MODELING

16. SECURITY CLASSIFICATION OF:			17. LIMITATION OF ABSTRACT	18. NUMBER OF PAGES	19a. NAME OF RESPONSIBLE PERSON
a. REPORT	b. ABSTRACT	c. THIS PAGE	UU	21	SOFI BIN-SALAMON
U	U	U			19b. TELEPHONE NUMBER *(include area code)* 703-696-8411

TABLE OF CONTENTS

ABSTRACT

Considering multifunctional fibrous composites, laminates and structures, a unified, transformation field analysis (TFA) approach is developed to model their overall response to thermomechanical loads, as well as local phenomena due to coupled effects and damage. Local stresses and strains generated as a result of piezoelectric and/or pyroelectric behavior of the fibers are treated as transformation fields, which remain in the system even under mechanical unloading. Their effect on the stress and strain distribution at the microscale of a unidirectional composite, the macroscale of a laminate, and the structural scale is determined in terms of transformation influence factors that are a function of the elastic properties of the fiber and matrix phases, and the geometry idealizations at the three length scales. Treatment of damage follows the same scheme but the transformation fields are instead determined such that the local stresses in the affected phase are removed. The result is tri-lengthscale model, which seamlessly connects the stress and strain fields in the fiber and matrix phases, membrane forces and bending moments in laminates, and the overall thermomechanical, structural loads to determine the overall response. The Mori-Tanaka and the periodic hexagonal array models were utilized to model the micromechanical behavior of the individual composite laminas, and the laminated plate theory was applied for fibrous laminates. The structural response is determined with the ABAQUS finite element code, in which the transformation field analysis was implemented as a user-defined routine. Examples are given for composite laminates and structures to illustrate the capabilities of the developed approach in predicting the overall behavior for multifunctional composite structures.

1. INTRODUCTION

In the rapidly developing field of multifunctional composites, robust modeling of laminated structures with piezoelectric fibers is lacking. There is a real need to combine analysis of large structural parts with realistic material models, which represent the underlying deformation phenomena. There is no shortage of work in multifunctional composites in general, but the focus has been mainly on finding effective properties, including mechanical, electrical, and electromechanical constants. Examples are found in the work of Chen (1994), Aboudi (2001), Berger et al. (2005), Kumar and Chakraborty (2009), and Challagulla and Georgiades (2011). On the other hand, a combination of micro and macro mechanical modeling of laminated plates with embedded piezoelectric fiber is presented by Cook and Vel (2012). They implemented PFC actuators composed of PZT-7A fibers embedded in an epoxy resin inducing shear deformation when actuated in the axial direction. Application of a beam bending composed of a PFC shear actuator embedded between two graphite/polymer substrates is found in their work. A 3D axisymmetric laminated shell with piezoelectric sensors and actuators is presented by Santos et al, (2006). The shell is subject to mechanical load and electrical potential on the external surface. They plotted relations between stresses and displacements, radial and axial, and the applied electrical potential and pressure. Other researchers focused on the implementation of multifunctional composite laminates in structural health monitoring. Diamanti and Soutis (2010) used PZT transducers to act as actuators and sensors to detect damage in a carbon fiber/epoxy laminate due to low velocity impact. Almost the same technique is used by Giurgiutiu and Soutis (2011). They enabled the piezoelectric wafer active sensors (PWAS) to detect damage in a composite laminate using Lamb waves. Huang et al, (2009) investigated numerically the effect of integrating a SHM sensor in a unidirectional glass fiber laminate on the onset of cracks in the resin matrix. The same problem is studies experimentally by Ghezzo et al. (2009). Similarly, Lissenden et al. (2009) embedded a linear array of piezoelectric fibers at the mid-plane of a carbon fiber reinforced polymer laminate. They simulated actuation of the PZT fibers by applying a radial displacement around their circumference and studied the effect on the elastic strain energy density of the system.

This work focuses on the micromechanical analysis of a structure made of a laminated composite with piezoelectric fibers. The analysis therefore includes the interaction between different length scales of the problem. From the broadest to the finest, there is a structure scale, a laminate scale, a composite scale and a phase scale. The structure scale is simulated using ABAQUS Explicit formulation while the laminate scale is modeled using a transformation filed analysis scheme. The composite aggregate is solved on the micromechanical scale using a representative volume element, which models a periodic hexagonal distribution of the fibers.

This report describes the above work, which was completed under AFOSR sponsorship. The report is organized as follows: Section 2 describes the tri-lengthscale structural analysis model, which combines micromechanics, a laminate theory, and the finite element method. Applications are given in Section 3. The report closes with conclusions in Section 4.

2. A TRI-LENGTHSCALE MODEL FOR MULTIFUNCTIONAL LAMINATED COMPOSITE STRUCTURES

Development of a tri-lengthscale model for multifunctional composites structures was developed in two steps. First, analysis of fibrous laminates with an underlying micromechanical model for piezoelectric laminas was developed for overall membrane forces and bending moments using a Transformation Field Analysis (TFA). This establishes a dual lengthscale model, which relates the overall response of a fibrous laminate to both the in-situ properties, and the local deformations. Taking this analysis to the next level involves the integration of the TFA for laminates with a finite element framework. The model is described in detail in two publications by the principal investigator (Bahei-El-Din and Micheal, 2012, 2013). A summary of the tri-lengthscale model with relevant equations is given in this section.

2.1. MICRO-SCALE MECHANICS OF A FIBROUS COMPOSITE

Considering a unidirectional lamina, and assuming that it consists of Q phases, each has a volume fraction υ_r, the phase stresses, $\boldsymbol{\sigma}_r$, and strains, $\boldsymbol{\varepsilon}_r$, are related to their overall counterparts $\bar{\boldsymbol{\sigma}}$, $\bar{\boldsymbol{\varepsilon}}$, relative to the lamina coordinate system $\bar{x}_k$, by:

$$\bar{\boldsymbol{\sigma}} = \sum_{r=1,Q} \upsilon_r \boldsymbol{\sigma}_r, \quad \bar{\boldsymbol{\varepsilon}} = \sum_{r=1,Q} \upsilon_r \boldsymbol{\varepsilon}_r. \tag{1}$$

Both the stresses and strains appearing in Eq. (1) are (6x1) matrices which list the independent components of their tensorial counterparts. Hence, $\boldsymbol{\sigma} = \left[\sigma_{11}, \sigma_{22}, \sigma_{33}, \sigma_{23}, \sigma_{31}, \sigma_{12}\right]$, and $\boldsymbol{\varepsilon} = [\varepsilon_{11}, \varepsilon_{22}, \varepsilon_{33}, 2\varepsilon_{23}, 2\varepsilon_{31}, 2\varepsilon_{12}]$.

Constitutive equations of the phases can be written as (Bahei-El-Din and Dvorak, 2000)

$$\boldsymbol{\sigma}_r = \boldsymbol{L}_r \boldsymbol{\varepsilon}_r + \boldsymbol{\lambda}_r, \quad \boldsymbol{\varepsilon}_r = \boldsymbol{M}_r \boldsymbol{\sigma}_r + \boldsymbol{\mu}_r. \tag{2}$$

Here, $\boldsymbol{L}_r$ and $\boldsymbol{M}_r = \boldsymbol{L}_r^{-1}$ are elastic stiffness and compliance of phase r. The first term in Eq. (2) represents the response to mechanical loads and the second term represents the transformation or eigen fields, $\boldsymbol{\mu}_r$ and $\boldsymbol{\lambda}_r = -\boldsymbol{L}_r \boldsymbol{\mu}_r$, caused by effects other than mechanical loading. Examples of the latter are thermal changes and electrical fields induced to piezoelectric phases. The phases are assumed to be transversely isotropic. In terms of Hill's elastic moduli (Hill, 1964) the elastic stiffness matrix $\boldsymbol{L}_r$ is given by

$$\boldsymbol{L}_r = \begin{bmatrix} k+m & k-m & \ell & 0 & 0 & 0 \\ k-m & k+m & \ell & 0 & 0 & 0 \\ \ell & \ell & n & 0 & 0 & 0 \\ 0 & 0 & 0 & p & 0 & 0 \\ 0 & 0 & 0 & 0 & p & 0 \\ 0 & 0 & 0 & 0 & 0 & m \end{bmatrix}. \tag{3}$$

In terms of engineering moduli, Hill's moduli are given by:

$$k=-\left[\frac{1}{G_T}-\frac{4}{E_T}+\frac{4\nu_L^2}{E_L}\right],\quad \ell=2k\nu_L,\ n=E_L+4k\nu_L^2=E_L+\ell^2/k,\quad m=G_T,\quad p=G_L, \tag{4}$$

where E_L, E_T are longitudinal and transverse Young's moduli, ν_L is Poisson's ratio corresponding to axial straining, and G_L, G_T are longitudinal and transverse shear moduli.

In analogy with (2), the following constitutive relations can be written for the lamina relative to the material principal axes $\bar{x}_k$,

$$\bar{\boldsymbol{\sigma}}=\bar{\boldsymbol{L}}\bar{\boldsymbol{\varepsilon}}+\bar{\boldsymbol{\lambda}},\quad \bar{\boldsymbol{\varepsilon}}=\bar{\boldsymbol{M}}\bar{\boldsymbol{\sigma}}+\bar{\boldsymbol{\mu}}, \tag{5}$$

where $\bar{\boldsymbol{L}}$ and $\bar{\boldsymbol{M}}=\bar{\boldsymbol{L}}^{-1}$ are overall elastic stiffness and compliance. The lamina is transversely isotropic and as such the overall elastic stiffness can be written as given in Eq. (3) in terms of overall moduli which can be either measured or modeled (Bahei-El-Din and Dvorak, 2000).

The lamina transformation stress $\bar{\boldsymbol{\lambda}}$ and strain $\bar{\boldsymbol{\mu}}$ can be expressed in terms of their local counterparts as (Dvorak and Benveniste, 1992)

$$\bar{\boldsymbol{\lambda}}=\sum_{r=1,Q}\upsilon_r\boldsymbol{A}_r^T\boldsymbol{\lambda}_r,\quad \bar{\boldsymbol{\mu}}=\sum_{r=1,Q}\upsilon_r\boldsymbol{B}_r^T\boldsymbol{\mu}_r, \tag{6}$$

where $\boldsymbol{A}_r$ and $\boldsymbol{B}_r$ are strain and stress concentration factors, which provide the phase fields in terms of their overall counterparts. These can be determined from a material model.

Considering overall mechanical loads together with local transformation fields, the strains and stresses in the phases of a unidirectional lamina can be expressed as (Dvorak, 1992)

$$\boldsymbol{\varepsilon}_r=\boldsymbol{A}_r\bar{\boldsymbol{\varepsilon}}+\sum_{s=1,Q}\boldsymbol{D}_{rs}\boldsymbol{\mu}_s, \tag{7}$$

$$\boldsymbol{\sigma}_r=\boldsymbol{B}_r\bar{\boldsymbol{\sigma}}+\sum_{s=1,Q}\boldsymbol{F}_{rs}\boldsymbol{\lambda}_s,\quad r=1,Q. \tag{8}$$

Here, $\boldsymbol{F}_{rs}$ and $\boldsymbol{D}_{rs}$ represent stress and the strain influence functions.

The phase transformation fields, $\boldsymbol{\lambda},\boldsymbol{\mu}$, appearing in Eqs. (2), (6-8) are generally caused by local phenomena in response to other induced fields. Considering a piezo/pyro-electrically active phase subjected to electrical field $\mathfrak{E}$ and temperature change θ, the transformation stresses and strains caused in this phase can be written as ,

$$\boldsymbol{\lambda}=-\boldsymbol{e}^T\mathfrak{E}-\boldsymbol{L}\boldsymbol{\alpha}\theta,\quad \boldsymbol{\mu}=\boldsymbol{d}^T\mathfrak{E}+\boldsymbol{\alpha}\theta, \tag{9}$$

where $\boldsymbol{\alpha}$ is the coefficient of thermal expansion, and $\boldsymbol{e}, \boldsymbol{d}$, denote piezoelectric constants. For transverse isotropy with x_3 the axis of rotational, they take the following form (Bahei-El-Din, 2009; Chen, 1994)

$$\boldsymbol{d}^{\mathrm{T}} = \begin{bmatrix} 0 & 0 & d_{31} \\ 0 & 0 & d_{31} \\ 0 & 0 & d_{33} \\ 0 & d_{15} & 0 \\ d_{15} & 0 & 0 \\ 0 & 0 & 0 \end{bmatrix}, \quad \boldsymbol{e}^{\mathrm{T}} = \begin{bmatrix} 0 & 0 & e_{31} \\ 0 & 0 & e_{31} \\ 0 & 0 & e_{33} \\ 0 & e_{15} & 0 \\ e_{15} & 0 & 0 \\ 0 & 0 & 0 \end{bmatrix}, \quad \boldsymbol{\alpha} = \begin{Bmatrix} \alpha_{\boldsymbol{T}} \\ \alpha_{\boldsymbol{T}} \\ \alpha_{\boldsymbol{L}} \\ 0 \\ 0 \\ 0 \end{Bmatrix}. \tag{10}$$

where α_L and α_T denote longitudinal and transverse coefficient of thermal expansion, respectively. The piezoelectric constants are related by (Bahei-El-Din, 2009)

$$e_{31} = 2kd_{31} + \ell d_{33}, \quad e_{33} = 2\ell d_{31} + nd_{33}, \quad e_{15} = pd_{15}. \tag{11}$$

The formulation is completed by listing the electric displacement $\mathcal{D}$ and electrical field $\mathcal{E}$ as the superposition of the direct effect and the coupling effects,

$$\mathcal{D} = \boldsymbol{\kappa}_{\varepsilon}\mathcal{E} + \boldsymbol{e}\boldsymbol{\varepsilon} - \boldsymbol{q}\theta = \boldsymbol{\kappa}_{\sigma}\mathcal{E} + \boldsymbol{d}\boldsymbol{\sigma} - \boldsymbol{q}\theta, \tag{12}$$

$$\mathcal{E} = \boldsymbol{\kappa}_{\sigma}^{-1}\mathcal{D} - \boldsymbol{g}\boldsymbol{\sigma} + \boldsymbol{h}\theta, \tag{13}$$

such that,

$$\boldsymbol{g} = \boldsymbol{\kappa}_{\sigma}^{-1}\boldsymbol{d}, \quad \boldsymbol{h} = \boldsymbol{\kappa}_{\sigma}^{-1}\boldsymbol{q} \tag{14}$$

Here, $\boldsymbol{g}$ is the voltage constant, $\boldsymbol{\kappa}_{\sigma}$ and $\boldsymbol{\kappa}_{\varepsilon}$ are (3x3) permittivity matrices measured at constant stress or constant strain, respectively, and $\boldsymbol{q}$ is pyroelectric constant. The piezoelectric constants are inter-related by (Bahei-El-Din, 2009)

$$g_{31} = d_{31} / \kappa_{33\sigma}, \quad g_{33} = d_{33} / \kappa_{33\sigma}, \quad g_{15} = d_{15} / \kappa_{11\sigma}. \tag{15}$$

For a transversely isotropic phase, the permittivity and the pyroelectric constant take the form (Chen, 1994; Kumar, 2009)

$$\boldsymbol{\kappa} = \begin{bmatrix} \kappa_{11} & 0 & 0 \\ 0 & \kappa_{11} & 0 \\ 0 & 0 & \kappa_{33} \end{bmatrix}, \quad q = \begin{Bmatrix} 0 \\ 0 \\ \mathrm{q}_3 \end{Bmatrix}. \tag{16}$$

2.2. MACRO-SCALE MECHANICS OF A FIBROUS LAMINATE

The laminate considered consists of n unidirectionally reinforced fibrous composite laminas with a total thickness h and lamina thickness t_i, $i=1,..n$. Hence, $\sum_{i=1,n} t_i = h$ and the lamina volume fraction is $c_i = t_i / h$. The global system of coordinates of the laminate is denoted by x_j, $j=1,2,3$, where $x_1 x_2$ is mid-plane of the laminate and x_3 is the out of plane direction. The laminas local coordinate system is denoted by $\bar{x}_k$, $k=1,2,3$, where the fibers are aligned in the $\bar{x}_3$ direction as shown in Fig. 1. The fiber orientation is specified by the angle, φ, between the $\bar{x}_3$ and x_1 axes. The laminate is subjected to membrane forces $\mathcal{N} = \left[\mathcal{N}_{11}, \mathcal{N}_{22}, \mathcal{N}_{12}\right]$ and bending moments $\mathcal{M} = \left[\mathcal{M}_{11}, \mathcal{M}_{22}, \mathcal{M}_{12}\right]$. In addition, the laminas may be subjected to a change of temperature θ. On the phase scale, fibers may possess a three-way, thermo-electro-mechanical coupling in response to the above mentioned mechanical loads and thermal change in addition to an electric field intensity $\mathcal{E} = \left(\mathcal{E}_1, \mathcal{E}_2, \mathcal{E}_3\right)$.

The membrane forces $\mathcal{N} = \left[\mathcal{N}_{11}, \mathcal{N}_{22}, \mathcal{N}_{12}\right]$ and bending moments $\mathcal{M} = \left[\mathcal{M}_{11}, \mathcal{M}_{22}, \mathcal{M}_{12}\right]$ applied to a fibrous laminate (Fig. 1) can be related to the stresses caused in the individual laminas as follows (Bahei-El-Din et al., 2010),

$$\mathcal{N} = \int_{-h/2}^{h/2} \hat{\boldsymbol{\sigma}}(z)\,dz = \sum_{i=1,n} \left(\int_{z_i - t_i/2}^{z_i + t_i/2} \hat{\boldsymbol{\sigma}}(z)\,dz \right), \tag{17}$$

$$\mathcal{M} = \int_{-h/2}^{h/2} z\,\hat{\boldsymbol{\sigma}}(z)\,dz = \sum_{i=1,n} \left(\int_{z_i - t_i/2}^{z_i + t_i/2} z\,\hat{\boldsymbol{\sigma}}(z)\,dz \right). \tag{18}$$

Equations (17,18) are written with reference to the global coordinate system x_j, $j=1,2,3$ shown in Fig. 1, where z refers to the x_3 coordinate of the midplane of a lamina. Symbols decorated with a top hat denote a list of in-plane components. Hence, the lamina stress vector appearing in Eqs. (17, 18) is written as $\hat{\boldsymbol{\sigma}} = \left[\sigma_{11}, \sigma_{22}, \sigma_{12}\right]$.

In-plane strains $\hat{\boldsymbol{\varepsilon}}(z) = [\varepsilon_{11}, \varepsilon_{22}, 2\varepsilon_{12}]$ are assumed to vary linearly across the laminate thickness (Bahei-El-Din et al., 2010). Hence,

$$\hat{\boldsymbol{\varepsilon}}(z) = \boldsymbol{\varepsilon}_o + z\,\boldsymbol{\kappa}, \tag{19}$$

where $\boldsymbol{\varepsilon}_o = [\varepsilon_{11}^o, \varepsilon_{22}^o, 2\varepsilon_{12}^o]$ and $\boldsymbol{\kappa} = [\kappa_1, \kappa_2, \kappa_{12}]$ are the strain and curvature at the mid-plane of the laminate, respectively. They are related to the applied loads by (Bahei-El-Din et al., 2010):

$$\boldsymbol{\varepsilon}_o = \mathcal{A}'\mathcal{N} + \mathcal{B}'\mathcal{M} + \boldsymbol{f}', \tag{20}$$

$$\boldsymbol{\kappa} = \boldsymbol{\mathcal{C}}'\boldsymbol{\mathcal{N}} + \boldsymbol{\mathcal{D}}'\boldsymbol{\mathcal{M}} + \boldsymbol{g}'. \tag{21}$$

The first two terms in Eqs. (20, 21) represent the contribution of the mechanical loads. The third term represents the effects caused by the lamina eignstresses.

Matrices $\boldsymbol{\mathcal{A}}', \boldsymbol{\mathcal{B}}', \boldsymbol{\mathcal{C}}', \boldsymbol{\mathcal{D}}', \boldsymbol{f}', \boldsymbol{g}'$ are a function of the elastic properties of the laminas, their volume fractions and laminate layup (Bahei-El-Din et al., 2010);

$$\boldsymbol{\mathcal{A}}' = (\boldsymbol{I} - \boldsymbol{\mathcal{B}}'\boldsymbol{\mathcal{B}})\boldsymbol{\mathcal{A}}^{-1}, \quad \boldsymbol{\mathcal{B}}' = -\boldsymbol{\mathcal{A}}^{-1}\boldsymbol{\mathcal{B}}\boldsymbol{\mathcal{D}}', \tag{22}$$

$$\boldsymbol{\mathcal{C}}' = -\boldsymbol{\mathcal{D}}'\boldsymbol{\mathcal{B}}\boldsymbol{\mathcal{A}}^{-1}, \quad \boldsymbol{\mathcal{D}}' = [\boldsymbol{\mathcal{D}} - \boldsymbol{\mathcal{B}}\boldsymbol{\mathcal{A}}^{-1}\boldsymbol{\mathcal{B}}]^{-1}, \tag{23}$$

$$\boldsymbol{f}' = -\boldsymbol{\mathcal{B}}'\boldsymbol{g} - \boldsymbol{\mathcal{A}}'\boldsymbol{f}, \quad \boldsymbol{g}' = -\boldsymbol{\mathcal{C}}'\boldsymbol{f} - \boldsymbol{\mathcal{D}}'\boldsymbol{g}, \tag{24}$$

where $\boldsymbol{\mathcal{A}}, \boldsymbol{\mathcal{B}}, \boldsymbol{\mathcal{D}}, \boldsymbol{f}, \boldsymbol{g}$ are related to lamina properties by;

$$\boldsymbol{\mathcal{A}} = \sum_{i=1,n} t_i \hat{\boldsymbol{L}}_i, \quad \boldsymbol{\mathcal{B}} = \sum_{i=1,n} (t_i z_i) \hat{\boldsymbol{L}}_i, \tag{25}$$

$$\boldsymbol{\mathcal{D}} = \sum_{i=1,n} t_i \left(\frac{1}{12} t_i^2 + z_i^2 \right) \hat{\boldsymbol{L}}_i, \tag{26}$$

$$\boldsymbol{f} = \sum_{i=1,n} t_i \boldsymbol{\lambda}_i, \quad \boldsymbol{g} = \sum_{i=1,n} (t_i z_i) \boldsymbol{\lambda}_i. \tag{27}$$

The (3x3) lamina stiffness matrix $\hat{\boldsymbol{L}}$ can be expressed in terms of Hill's overall elastic moduli of a unidirectional composite as follows (Bahei-El-Din, 1992),

$$\hat{\boldsymbol{L}} = \frac{1}{k+m} \begin{bmatrix} 4km & 2m\ell & 0 \\ 2m\ell & E_L k + mn & 0 \\ 0 & 0 & p(k+m) \end{bmatrix}. \tag{28}$$

In analogy with Eq. (8), lamina stresses in the overall coordinates x_j, are written as the superposition of the stresses caused by the laminate loads and those caused by the lamina transformation stresses;

$$\hat{\boldsymbol{\sigma}}_i = \boldsymbol{P}_i \boldsymbol{\mathcal{N}} + \boldsymbol{Q}_i \boldsymbol{\mathcal{M}} + \sum_{j=1,n} \boldsymbol{U}_{ij} \hat{\boldsymbol{\lambda}}_j. \tag{29}$$

Here, $\boldsymbol{P}_i$, $\boldsymbol{Q}_i$ denote stress distribution factors, and $\boldsymbol{U}_{ij}$ denotes stress transformation influence functions. They are a function of elastic moduli and volume fractions of the laminas, and the laminate layup (Bahei-El-Din et al., 2010);

$$\boldsymbol{P}_i = \hat{\boldsymbol{L}}_i \left(\boldsymbol{\mathcal{A}}' + z_i \boldsymbol{\mathcal{C}}' \right), \ \boldsymbol{Q}_i = \hat{\boldsymbol{L}}_i \left(\boldsymbol{\mathcal{B}}' + z_i \boldsymbol{\mathcal{D}}' \right), \tag{30}$$

$$\boldsymbol{U}_{ij} = \delta_{ij} \boldsymbol{I} - t_j \boldsymbol{P}_i - \left(t_j z_j \right) \boldsymbol{Q}_i . \tag{31}$$

Equilibrium of lamina forces leads to the following relations (Bahei-El-Din et al., 2010):

$$\sum_{i=1,n} t_i \boldsymbol{P}_i = \boldsymbol{I}, \qquad \sum_{i=1,n} \left(t_i z_i \right) \boldsymbol{P}_i = \boldsymbol{0}, \tag{32}$$

$$\sum_{i=1,n} t_i \boldsymbol{Q}_i = \boldsymbol{0}, \qquad \sum_{i=1,n} \left(t_i z_i \right) \boldsymbol{Q}_i = \boldsymbol{I}. \tag{33}$$

For completeness, coordinate transformation for the lamina stresses and strains are listed as follows (Bahei-El-Din et al., 2010):

$$\begin{aligned} &\hat{\bar{\boldsymbol{\sigma}}}_i = \boldsymbol{R}_i \hat{\boldsymbol{\sigma}}_i , \quad \hat{\bar{\boldsymbol{\varepsilon}}}_i = \boldsymbol{N}_i \hat{\boldsymbol{\varepsilon}}_i , \quad \hat{\bar{\boldsymbol{\lambda}}}_i = \boldsymbol{R}_i \hat{\boldsymbol{\lambda}}_i , \quad \hat{\bar{\boldsymbol{\mu}}}_i = \boldsymbol{N}_i \hat{\boldsymbol{\mu}}_i , \\ &\hat{\boldsymbol{L}}_i = \boldsymbol{N}_i^T \hat{\bar{\boldsymbol{L}}}_i \boldsymbol{N}_i , \quad \hat{\boldsymbol{M}}_i = \boldsymbol{R}_i^T \hat{\bar{\boldsymbol{M}}}_i \boldsymbol{R}_i , \end{aligned} \tag{34}$$

$$\boldsymbol{R}_i^T = \boldsymbol{N}_i^{-1} = \begin{bmatrix} \cos^2 \varphi_i & \sin^2 \varphi_i & -\frac{1}{2} \sin 2\varphi_i \\ \sin^2 \varphi_i & \cos^2 \varphi_i & \frac{1}{2} \sin 2\varphi_i \\ \sin 2\varphi_i & -\sin 2\varphi_i & \cos 2\varphi_i \end{bmatrix}, \tag{35}$$

where vectors decorated with a top bar are referred to the lamina material axes, otherwise reference is made to the laminate overall coordinates, and φ_i denotes the fiber orientation, Fig. 1.

2.3. GLOBAL-SCALE ANALYSIS OF FIBROUS COMPOSITE STRUCTURES

In utilizing the transformation field analysis for composites in explicit formulation of the finite element method, it is essential to note the analogy between treatment of the latter for non-mechanical deformations, e.g. thermal strains, and the TFA formulation. In both cases, the structure is treated as elastic, with superimposed deformations stemming from the non-mechanical fields. In the present problem for piezoelectric composites, the non-mechanical strain and stresses are due to electromechanical coupling of the phases. Hence, in implementing the TFA analysis into any finite element framework, the eigen stresses are computed with the above formulation and its underlying micromechanical model and used to update the nodal loads.

For an eigen stress $\boldsymbol{\lambda}_m$ found in a laminated composite element of a finite element mesh, which represents some structure, the nodal forces $\boldsymbol{q}_m$, which equilibrate the eigen stresses are given by the principle of virtual work,

$$\boldsymbol{q}_m = \int_{V_m} \boldsymbol{\Gamma}_m \boldsymbol{\lambda}_m dV_m \,, \tag{36}$$

Where $\boldsymbol{\Gamma}_m$ represents spatial derivatives of the displacement field in element m, and V_m is volume of the element.

The entire TFA model is coded into the user defined subroutine UEXPAN of the ABAQUS finite element program. This serves as the interface between the global finite element mesh and the response of the individual elements. The latter are symmetric laminates for which the eigen strains and stresses are calculated with the TFA method described in Sections 2.1 and 2.2 and supplied to the finite element scheme.

3. RESULTS

In preparation for a finite element analysis of a laminated structure, the TFA scheme is used first to prepare the data required in the finite element solution, namely the overall elastic properties of the laminate, and the data required for the transformation field analysis, namely the stress and strain concentration factors and influence functions. In this pre-processing stage, a micromechanical model is to be utilized for the micromechanical formulation of Section 2.1. In the present work, a refined, periodic hexagonal array (PHA) model (Dvorak and Teply, 1985) is applied. In this case, a representative volume element (RVE) is divided into subvolumes V_r, $r = 1, Q$, and analyzed under certain loads, which are derived from eqs. (7, 8) to compute the columns of the concentration factors $\boldsymbol{A}_r$, $\boldsymbol{B}_r$, and influence functions $\boldsymbol{D}_{rs}$, $\boldsymbol{F}_{rs}$, $r, s = 1, Q$.

Two applications are presented; one is a benchmark, classical laminated plate problem, and one which involves a laminated plate with complex geometry. In both problems the unidirectional composite used consists of piezoelectric fibers (PZT-5A) embedded in an epoxy (DY-063) matrix. The mechanical properties of both constituents are given in Table 1, and electrical properties of the fibers are given in Table 2. The fiber volume fraction is kept at 0.55 for all plies. Using the laminated plate analysis (Section 2.2) with the unidirectional plies represented by the PHA model and an RVE with 60 fiber subvolumes and 240 matrix subvolumes, the overall elastic properties are determined for two symmetric laminates, a cross ply, $(0/90)_s$, and a quasi-isotropic, $(0/\pm45/90)_s$ laminate. The results are given in Table 3.

3.1. BENCHMARK PROBLEMS

To verify that the tri-lengthscale analysis using TFA/ABAQUS yields the same results as the stand alone TFA, a solid plate constructed from a $(0/90)_s$ laminate is considered. The electrically active fibers in the 0^o lamina are subjected to an electric field $\mathcal{E}_3$ in the axial direction at a magnitude of $1.0\text{x}10^6$ V/m. This induces eigen stresses $\lambda_{11} = \lambda_{22} = -e_{31}\mathcal{E}_3$, $\lambda_{33} = -e_{33}\mathcal{E}_3$ in the 0^o, PZT fiber, and the corresponding overall strain at mid-plane of the laminate is computed with the TFA scheme as $\varepsilon_{11} = 2.70\text{x}10^{-4}$, $\varepsilon_{22} = -5.11\text{x}10^{-5}$, and $\varepsilon_{12} = 0$. Using the ABAQUS finite element code, the same plate problem was solved, where the non-mechanical, eigen strains caused by the electric field in the 0^o, PZT fiber are computed through the user subroutine

UEXPAN with the TFA scheme. The plate, which measured 0.5x0.5 m, was subdivided into 25 quadrilateral elements of equal dimensions and was unconstrained at the boundaries. The finite element results obtained in this case were identical with those provided by the laminate analysis.

3.2. EXAMPLES

Consider a square, quasi-isotropic, $(0/\pm45/90)_s$ laminated plate with a concentric circular hole. The side length of the plate is 0.5 m, and diameter of the hole is 0.1 m. The tri-lengthscale TFA/ABAQUS model was used to solve the problem, where the underlying micromechanical model is the periodic hexagonal array. As indicated earlier, the overall elastic properties of the laminate together with the stress concentration factors and influence functions of the fiber and matrix subvolumes are pre-determined and stored for processing by the user-defined subroutine UEXPAN. The overall elastic properties of the quasi-isotropic laminate under consideration are given in Table 3.

In the finite element analysis one quarter of the plate was considered with boundary conditions which simulate symmetry of the overall deformations. In one problem, the plate is otherwise unconstrained and subjected to an overall tensile stress of 50 MPa in direction of the 0^o fiber. The stress contours obtained from ABAQUS for σ_{11}, the stress in direction of the load are shown in Fig. 2. In a post-processor exercise, the TFA approach was used to determine the local fields in the fiber and matrix within all laminas using the overall stresses found from the finite element analysis. In particular, the electric displacement generated in the PZT fiber within the 0^o lamina are of interest as it reflects the stress concentration caused by discontinuity of the plate geometry. This is indicated in Fig. 3, where values of the electric displacement at selected locations are shown as insets on the map for the overall stress in direction of the applied load. It is seen that the magnitude of the computed electric displacement reflects the stress gradient. It is worth mentioning that the electric displacement in the same laminated plate without the circular discontinuity at overall stress of 50 MPa is $6.3\text{x}10^{-2}$ C/m^2. The same magnitude is found in the plate under consideration at the upper-right corner where the stress field is closest to that found in the solid plate. On the other hand, the electric displacement found at perimeter of the circular cutout is 2.2 C/m^2 at the stress free, three-o'clock location. This is caused by the overall stress in the X_2 direction, which is transverse to the load. The electric displacement at the twelve-o'clock location where the stress concentration is the largest is 18.8 C/m^2.

In another loading condition, the PZT fiber in the 0^o plies is subjected to an electric field $\mathcal{E}_3$ of $1.0\text{x}10^6$ V/m in the longitudinal direction. In this problem, the boundary conditions are modified to impose a displacement constraint in the direction perpendicular to the outer edges of the plate in addition to the symmetry boundary conditions. Following a finite element analysis with the ABAQUS program with the TFA interface, post processing of the results provides the ply and phase stresses. To illustrate this capability of the presented tri-multiscale analysis, we list

in Table 4 the ply stresses, σ_{11}, σ_{22}, σ_{12}, and the fiber axial stress, σ_L^f, at locations where each of the overall stresses S_{11}, S_{22}, S_{12} is a maximum.

Additional post-processing of the finite element results using the micromechanical/laminate analysis of Sections 2.1 and 2.2 yields the electric displacement in the active fibers of the 0^o plies caused by the applied electrical field, $\mathcal{E}_3$, introduced in the same fiber. The electric displacement thus calculated is due to the overall stresses generated as a result of the plate geometry and constraints. When this is superimposed on the electric displacement due to (1) the direct electric effect, $\kappa_{33}\mathcal{E}_3$, and (2) the local stress generated as a result of the mutual constraints of the phases and plies, and the result is divided by the applied electric field, the apparent permittivity is obtained. Figure 4 shows the apparent permittivity at selected locations, superimposed on contours of the overall stress found in direction of the X_1 axis. We note that the permittivity is the smallest at the twelve-o'clock location at perimeter of the circular hole where the stress due to the electric field in the 0^o fiber is the largest. In contrast, the permittivity at the three-o'clock location is $9.6\text{x}10^{-9}$ C/V.m. As expected, this is close to that found in a laminated plate of the same geometry and material (Bahei-El-Din and Micheal, 2012).

4. CONCLUSIONS

A tri-lengthscale model for analysis of composite structures with piezoelectric constituents is presented. It combines a micromechanical model for fibrous composites, a laminated plate analysis under plane stress, and a finite element analysis. The micromechanical model utilized is a refined one in which the stress and strain fields in the fiber and matrix are represented by piecewise uniform idealizations. The finite element analysis was performed with the ABAQUS program. Non-mechanical stresses and strains generated in composite phases are treated as transformation (eigen) fields and their effect on the composite media is determined with a transformation field analysis.

The applications presented cover a benchmark problem, which verifies that the results of the tri-lengthscale TFA/ABAQUS model are reliable, and a plate with a hole, which illustrates the capabilities of the solution scheme in analyzing complex geometries with detailed underlying models. Extension of this solution strategy to other eigen fields, stemming for example from pyroelectric effects and damage, is quite feasible and currently in progress by the authors.

ACKNOWLEDGEMENTS

The authors gratefully acknowledge the support provided by AFOSR, Award No. FA9550-11-1-0076. Drs. David Stargel and Sofi Bin-Salamon served as monitors.

REFERENCES

Aboudi, J., 2001. Micromechanical analysis of fully coupled electro-magneto-thermo-elastic multiphase composites. *Smart Materials and Structures* **10**, 867-877.

Bahei-El-Din, Y.A., 1992. Uniform fields, yielding, and thermal hardening in fibrous composite laminates. *International Journal of Plasticity* **8**, 867-892.

Bahei-El-Din, Y.A., 2009. Modeling electromechanical coupling in woven composites exhibiting damage. *Proceedings of IMechE* **223**, Part G: J Aerospace Engineering, 485-495.

Bahei-El-Din, Y.A., Dvorak, G.J., 2000. Micromechanics of inelastic composite laminates, in Comprehensive Composite Materials, A. Kelly and C. Zweben, Editors-in-Chief, Chapter 15 in Volume 1: General Theory of Composites, edited by T.-W. Chou, Elsevier Science B.V., Amsterdam.

Bahei-El-Din, Y.A., Micheal, A., 2012. Micromechanical modeling of multifunctional composites. Proceedings of the International Mechanical Engineering Congress & Exposition. ASME 2012 IMECE, Paper No. 89304, November 9-15, 2012, Houston, Texas, USA.

Bahei-El-Din, Y.A., Micheal, A., 2013. Multiscale analysis of multifunctional composite structures. Proceedings of the International Mechanical Engineering Congress & Exposition. ASME 2012 IMECE, Paper No. 89304, November 13-21, 2013, San Diego, California, USA.

Bahei-El-Din, Y.A., Khire, R., Hajela, P., 2010. Multiscale transformation field analysis of progressive damage in fibrous laminates. *International Journal for Multiscale Computational Engineering* **8**, 69-80.

Berger, H., Kari S., Gabbert U., Rodriguez-Ramos, R., Guinovart, R., Otero, J.A., Bravo-Castillero, J., 2005. An analytical and numerical approach for calculating effective material coefficients of piezoelectric fiber composites. *International Journal of Solids and Structures* **42**, 5692-5714.

Berlincourt, D., Krueger, H.H.A., Near, C., 2009. Properties of MORGAN electro ceramic ceramics. www.morgan-electrocceramics.com.

Challagulla, K.S., Georgiades, A.V., 2011. Micromechanical analysis of magneto-electro-thermo-elastic composite materials with applications to multilayered structures. *International Journal of Engineering Science* **49**, 85-104.

Chen, T., 1994. Micromechanical estimates of the overall thermoelectroelastic moduli of multiphase fibrous composites. *International Journal of Solids and Structures* **31**, No. 22, 3099-3111.

Cook, C.A., Vel, S.S., 2012. Multiscale analysis of laminated plats with integrated piezoelectric fiber composite actuators. *Composite Structures* **94**, 322-336.

Diamanti, K., Soutis, C., 2010. Structural health monitoring techniques for aircraft composite structures. *Aerospace Sciences* **46**, 342-352.

Dvorak, G.J., 1992. Transformation field analysis of inelastic composite, *Proceedings of the Royal Society London* **A437**, 311-327.

Dvorak, G.J., Benveniste, Y., 1992. On transformation strains and uniform fields in multiphase elstic media. *Proceedings of the Royal Society London* **A437**, 291-310.

Dvorak, G.J., Teply, J.L., 1985. Periodic hexagonal array models for plasticity analysis of composite materials. *In A. Sawczuk and V. Bianchi (eds.), Plasticity Today: Modeling Methods and Applications, W. Olsazak Memorial volume, Elsevier scientific publishing Co., Amsterdam*, 623-642.

Ghezzo, F., Huang, Y., Nemat-Nasser S., 2009. Onset of resin micro-cracks in unidirectional glass fiber laminates with integrated SHM sensors: experimental results. *Structural Health Monitoring* **8**, 477-491.

Giurgiutiu, V., Soutis, C., 2011. Enhanced Composite integrity Through Structural Health Monitoring. *Applied Composite Materials* 19,813-829.

Hill, R., 1964. Theory of mechanical properties of fiber-strengthened materials: I. Elastic behavior. *Journal of the Mechanics and Physics of Solids* **12**, 199-212.

Huang, Y., Ghezzo, F., Nemat-Nasser, S., 2009. Onset of resin micro-cracks in unidirectional glass fiber laminates with integrated SHM sensors: numerical analysis. *Structural Health Monitoring* **8**(6), 493-507.

Kumar, A., Chakraborty, D., 2009. Effective properties of thermo-electro-mechanically coupled piezoelectric fiber reinforced composites. *Material and Design* **30**, 1216-1222.

Levin, V.M., 1967. Thermal expansion coefficients of heterogeneous materials. *Mechanics of Solids* **11**, 58–61.

Lissenden, C.J., Blackshire, J.L., Puthillath, P.K., 2009. Structural health monitoring of composite laminates with embedded piezoelectric fibers. *Review of Quantitative Nondestructive Evaluation* **28**, 974-981.

Santos, H., Soares C. M. M., Soares C. A. M., Reddy J.N., 2006. A finite element for the analysis of 3D axisymmetric laminated shells with piezoelectric sensors and actuators. *Composite Structures* **72**, 170-178.

LIST OF TABLES

LIST OF FIGURES

Table 1. Mechanical properties of the fiber and matrix (Bahei-El-Din, 2009; Berlincourt et al., 2009).

Material	E (GPa)	ν
PZT-5A	60	0.34
DY063 Epoxy	3.35	0.35

Table 2. Piezo/pyroelectric properties of PZT-5A fibers (Bahei-El-Din, 2009; Berlincourt et al., 2009).

d_{31}	d_{33}	d_{51}	g_{31}	g_{33}	g_{15}
(10^{-12} m/V)			(10^{-3} V.m/N)		
-171	347	584	11.4	24.8	38.2

Table 3. Computed overall mechanical properties of laminates.

Layup	E_{11} (GPa)	E_{22} (GPa)	G_{12} (GPa)	ν_{12}
$(0/90)_s$	22.37	22.37	3.69	0.15
$(0/\pm45/90)_s$	17.76	17.76	6.71	0.325

Table 4. Lamina and fiber stresses at locations of maximum overall stress components (MPa).

Overall Stress	Lamina	σ_{11}	σ_{22}	σ_{12}	σ_L^f
S_{11}	0^o	-14.60	-.21	0.48	-25.4
	45^o	-5.12	-1.10	-0.64	-6.02
	-45^o	-6.79	-2.77	-3.18	-13.5
	90^o	-3.86	-2.91	0.48	5.87
S_{12}	0^o	-9.58	-.57	1.08	-16.5
	45^o	-2.38	-.11	1.35	0.72
	-45^o	-6.12	-3.85	4.37	-16.1
	90^o	-2.64	.33	1.08	1.12
S_{22}	0^o	-1.06	1.28	0.02	-2.10
	45^o	0.65	2.01	0.69	3.36
	-45^o	0.57	1.92	-0.56	3.0
	90^o	0.05	4.87	0.02	8.46

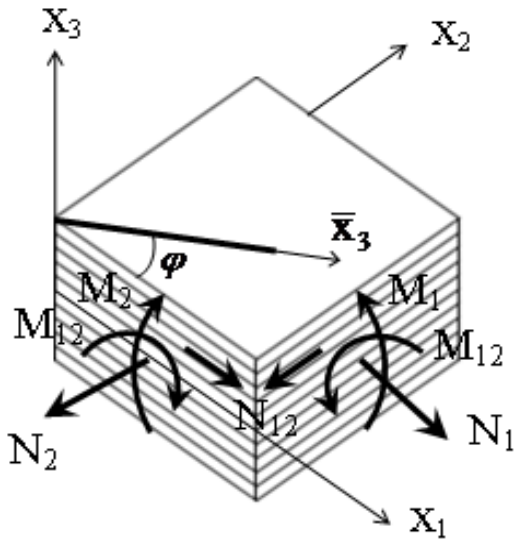

Fig. 1. Geometry and load of a fibrous laminate.

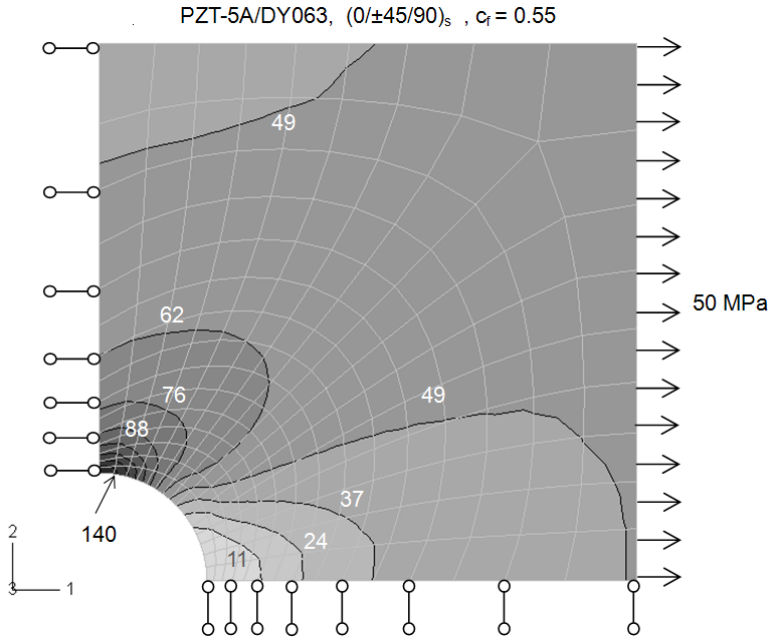

Fig. 2. Contours of σ_{11} stress (MPa) caused by an overall stress of 50 MPa in the X_1 direction.

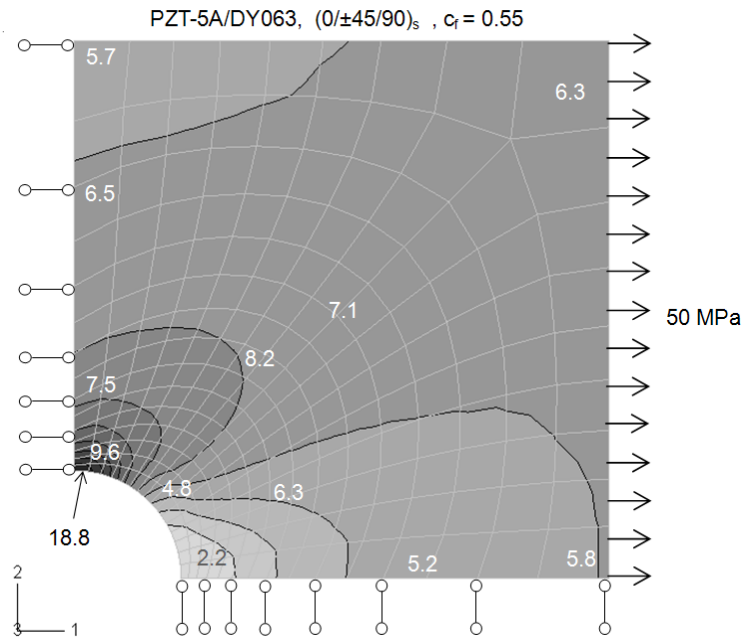

Fig. 3. Electric displacement $\mathcal{D}_3$ computed in 0^o PZT fiber (10^{-2} C/m^2) superimposed on σ_{11} stress contours (Fig. 2) at selected locations, due to an overall stress of 50 MPa in the X_1 direction.

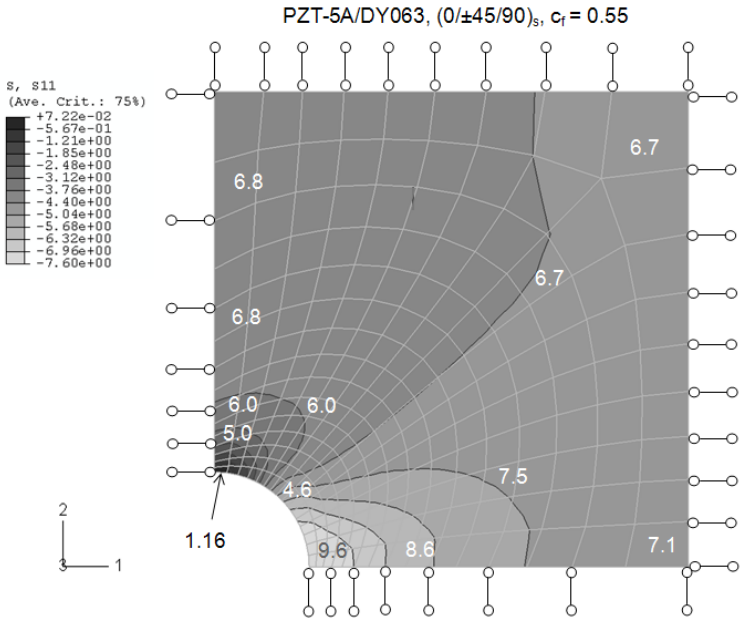

Fig. 4. Apparent permittivity computed in 0^o PZT fiber (10^{-2} C/V.m) superimposed on σ_{11} stress contours (MPa) at selected locations, due to electric field $\mathcal{E}_3$ of 1.0×10^6 V/m induced in the 0^o fiber.